Nucleotide immune signal activates bacterial caspase by filament depolymerization

Xuzichao Li[1,2,3#], Qiuqiu He[1,2#], Bin Liu[1,2#], Zhikun Liu[1,2#], Qian Zhang[1,2], Xiaoshen Wang[1,2], Tongyu Mao[1], Jie Han[1], Shuqin Zhang[1,2], Fumeng Liao[1], Yingcan Liu[1], Zhengda Shan[1,4], Zhenning Yin[1,2], Yong Wei[3], Zhiyong Yuan[4], Hang Yin[1], Heng Zhang[*1,2,4]

https://doi.org/10.15302/vita.2026.10.0084

Dear Editor,

Nucleotide immune signaling pathways rely on enzymatically generated second messengers to activate downstream effectors[1]. In bacterial type IV Thoeris systems, TIR enzymes convert NAD^+ into 5′-diphosphate-cyclo[N7:1′′]-ribose (N7-cADPR), which activates the caspase-like protease to confer population-level immunity during phage infection[2]. In striking contrast to human caspases, whose activation depends on proteolytic maturation, type IV Thoeris caspases are controlled by a nucleotide second messenger-mediated mechanism[2]. However, the molecular basis of N7-cADPR-dependent TIR-caspase activation in antiphage defense remains unknown. Here, we biochemically and structurally characterize the type IV Thoeris system from *Escherichia coli*. Our study reveals how nucleotide immune signal activates bacterial caspase through filament depolymerization, expanding our understanding of nucleotide immune pathways and prokaryotic defense strategies.

Type IV Thoeris locus from *Escherichia coli* encodes two protein components, including a TIR-domain protein (*Ec*TIR: aa 1–133) and a caspase-like protease (*Ec*Caspase: aa 1–321) (Fig. 1a). The protease harbors an N-terminal caspase-like domain (NTD: aa 1–231) that is naturally fused to a C-terminal domain of unknown function (CTD: aa 232–321). We first cloned the complete type IV Thoeris operon under a pBAD promoter and assessed its antiviral activity against a panel of phages in *Escherichia coli*. This system conferred strong resistance to various types of phages, with the strongest resistance against the T6 phage (Fig. 1b). RT-qPCR analysis revealed that *Ec*Caspase expression was upregulated upon phage infection (Supplementary Fig. S1). Catalytic mutants in either *Ec*TIR (E84Q) or the *Ec*Caspase (C132A) abolished protection, demonstrating that the activities of both enzymes are critical for anti-phage defense (Fig. 1c). Consistent with previous reports that the *Ec*Caspase exhibits proteolysis activity[2], our fluorescence-based peptide assays confirmed this activity, supporting the notion that *Ec*Caspase-mediated proteolytic cleavage underlies antiphage defense (Fig. 1d, e; Supplementary Fig. S2). Strikingly, negative-stain analyses of both MBP-fused and tag-free purified wild-type (WT) *Ec*Caspase revealed the formation of long, continuous filaments ranging from several tens to hundreds of nanometers in length (Supplementary Fig. S3a, b). Moreover, *Ec*Caspase readily forms filaments even at low concentrations (Supplementary Fig. S3c), whereas higher concentrations markedly increase filament length, consistent with a concentration-regulated assembly process. In contrast, these assemblies dissociate into low-order oligomers in the presence of N7-cADPR, regardless of the MBP-fused or tag-free *Ec*Caspase (Supplementary Fig. S3a, b). Consistently, native PAGE analysis of GFP-tagged *Ec*Caspase in *E. coli* showed that phage infection shifted *Ec*Caspase from high-molecular-weight assemblies retained on the top of the gel to migrating species, suggesting an assembly–to–disassembly transition *in vivo* (Supplementary Fig. S3d). Thus, it seems that the type IV Thoeris *Ec*Caspase follows a ligand-triggered depolymerization-activation mechanism, switching from a filamentous, likely inhibitory state to an active state upon N7-cADPR binding.

To elucidate the molecular basis of filament formation, we performed cryo-EM analysis of both MBP-fused and tag-free *Ec*Caspase in the absence of N7-cADPR (Supplementary Figs. S4, S5). Both structures exhibit highly similar overall architectures and protomer conformations (Supplementary Fig. S5e). Due to the well-defined density, we focused subsequent structural analyses on the MBP-fused *Ec*Caspase structure unless otherwise noted. The filament displays a pseudo-C4 point-group symmetry: the CTDs stack to form a compact central core, while the NTDs wrap helically around this core, resembling a spiraling dragon coiling around a pillar (Fig. 1f, g; Supplementary Fig. S6a). *Ec*Caspase protomer adopts a bilobed, dumbbell-like architecture comprising an NTD part and a CTD region, likely to mediate ligand engagement (Supplementary Fig. S6b–d). In the filament structure, two *Ec*Caspase protomers constitute a dimeric asymmetric unit (ASU) (Fig. 1h). These dimer units assemble into a right-handed helix with a rotation of 90° per ASU and an axial rise of 22.9 Å, yielding a helical pitch of ~91.6 Å per turn (Fig. 1f).

1. State Key Laboratory of Experimental Hematology, Tianjin Medical University Cancer Institute and Hospital, Key Laboratory of Immune Microenvironment and Disease (Ministry of Education), The Province and Ministry Co-Sponsored Collaborative Innovation Center for Medical Epigenetics, National Clinical Research Center for Cancer, Tianjin Institute of Immunology, Tianjin's Clinical Research Center for Cancer, School of Basic Medical Sciences, Tianjin Medical University, Tianjin, China. 2. Tianjin Key Laboratory of Cellular Homeostasis and Disease, Key Laboratory of Cancer Prevention and Therapy, Department of Biochemistry and Molecular Biology, Tianjin Medical University, Tianjin, China. 3. Hangzhou Institute of Medicine, Chinese Academy of Sciences, Hangzhou, Zhejiang, China. 4. Department of Radiation Oncology, Tianjin Medical University Cancer Institute and Hospital, National Clinical Research Center for Cancer, Key Laboratory of Cancer Prevention and Therapy, Tianjin's Clinical Research Center for Cancer, Tianjin, China. #These authors contribute equally. *Correspondence: Heng Zhang (zhangheng134@gmail.com)

Received: February 24, 2026; Accepted: September 21, 2026; Published: November 18, 2026

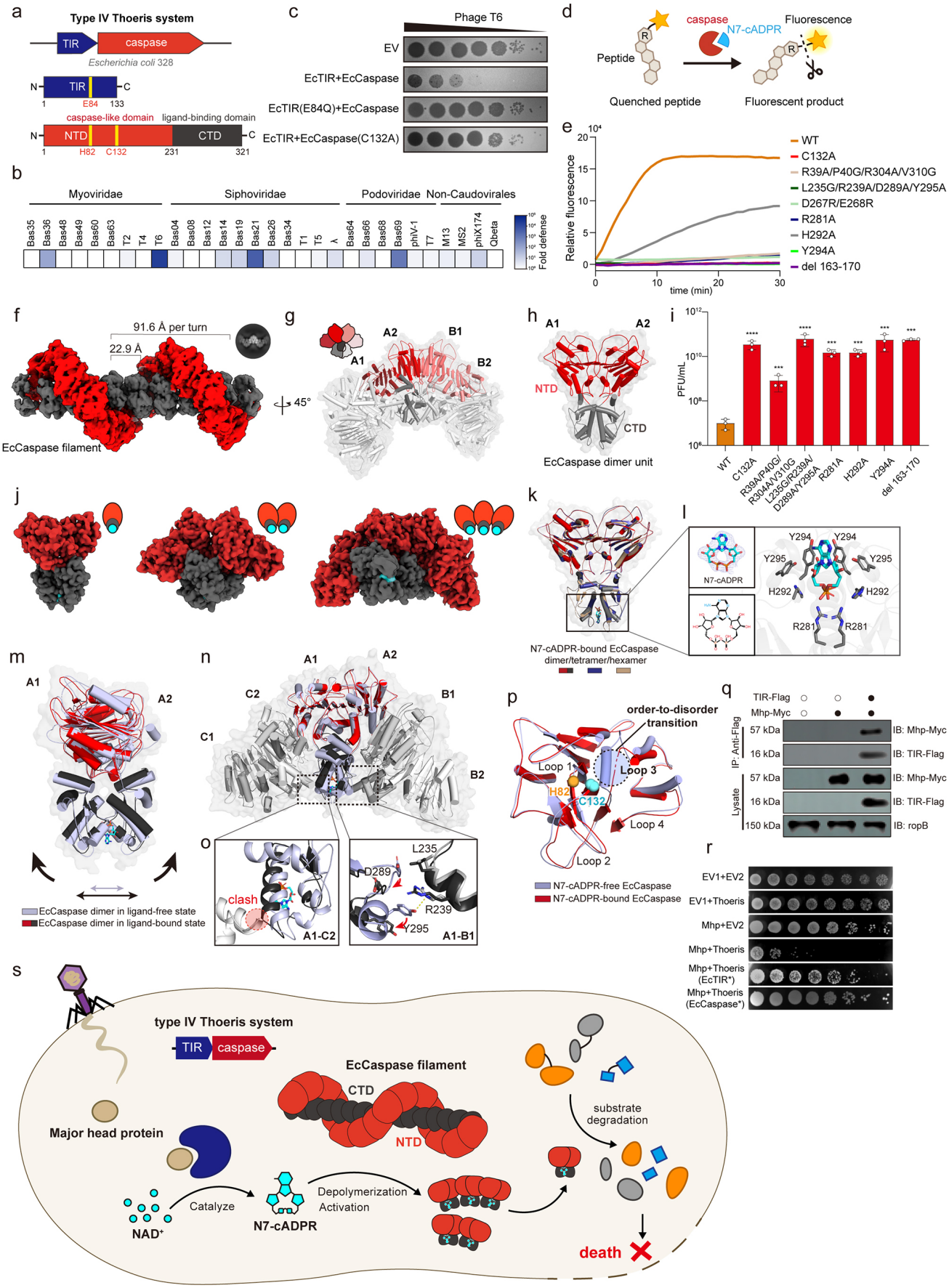

a
Type IV Thoeris system
TIR
caspase
Escherichia coli 328
N
TIR
C
1
E84
133
caspase-like domain
ligand-binding domain
NTD
CTD
H82
C132
231
321
b
Myoviridae
Siphoviridae
Podoviridae
Non-Caudovirales
Bas35 Bas36 Bas48 Bas49 Bas60 Bas63 T2 T4 T6 Bas04 Bas08 Bas12 Bas14 Bas19 Bas21 Bas26 Bas34 T1 T5 λ Bas64 Bas66 Bas68 Bas69 phiV-1 T7 M13 MS2 phiX174 Qbeta
Fold defense
c
Phage T6
EV
EcTIR+EcCaspase
EcTIR(E84Q)+EcCaspase
EcTIR+EcCaspase(C132A)
d
Peptide
caspase
N7-cADPR
Fluorescence
Quenched peptide
Fluorescent product
e
Relative fluorescence
time (min)
WT
C132A
R39A/P40G/R304A/V310G
L235G/R239A/D289A/Y295A
D267R/E268R
R281A
H292A
Y294A
del 163-170
f
91.6 Å per turn
22.9 Å
EcCaspase filament
g
45°
A1
A2
B1
B2
h
NTD
CTD
EcCaspase dimer unit
i
PFU/mL
WT
C132A
R39A/P40G/R304A/V310G
L235G/R239A/D289A/Y295A
D267R/E268R
R281A
H292A
Y294A
del 163-170
j
k
N7-cADPR-bound EcCaspase dimer/tetramer/hexamer
l
N7-cADPR
Y294
Y295
H292
R281
m
EcCaspase dimer in ligand-free state
EcCaspase dimer in ligand-bound state
n
C1
C2
o
clash
A1-C2
L235
D289
R239
Y295
A1-B1
p
order-to-disorder transition
Loop 1
Loop 2
Loop 3
Loop 4
H82
C132
N7-cADPR-free EcCaspase
N7-cADPR-bound EcCaspase
q
TIR-Flag
Mhp-Myc
IP: Anti-Flag
Lysate
57 kDa
16 kDa
150 kDa
IB: Mhp-Myc
IB: TIR-Flag
IB: ropB
r
EV1+EV2
EV1+Thoeris
Mhp+EV2
Mhp+Thoeris
Mhp+Thoeris (EcTIR*)
Mhp+Thoeris (EcCaspase*)
s
type IV Thoeris system
TIR
caspase
EcCaspase filament
CTD
NTD
Major head protein
Catalyze
NAD+
N7-cADPR
Depolymerization
Activation
substrate degradation
death

Fig. 1 Mechanism of *Ec*Caspase filament disassembly and activation induced by N7-cADPR binding. a Gene architecture of the type IV Thoeris system from *E. coli* 328. Domain architectures of caspase-like and *Ec*TIR proteins are shown. **b** Heatmap showing fold defense of *E. coli* expressing the type IV Thoeris system against the indicated phages. Fold defense was measured through serial dilution spot tests. **c** Plaque assays of T6 phage on lawns of strain MG1655 cells expressing wild-type or catalytic-dead type IV Thoeris system. EV, empty vector. Data are representative of three independent experiments. **d** Schematic of the *Ec*Caspase peptide cleavage reporter assays. **e** Peptide-cleavage reporter assays of *Ec*Caspase and its mutants in the presence of N7-cADPR. Data are representative of three independent experiments. **f, g** Cryo-EM map (**f**) and atomic model (**g**) of *Ec*Caspase filaments. **h** Atomic model of the represented asymmetric unit of the *Ec*Caspase filaments. **i** PFU quantification of *Ec*Caspase variants with mutations participating in N7-cADPR binding. Data represent mean ± SD from three biological replicates. Statistical significance was determined using unpaired two-tailed Welch's *t*-tests on $\log_{10}$-transformed PFU values, with each variant compared with WT. ns, $P \geq 0.05$; $^{*}P < 0.05$; $^{**}P < 0.01$; $^{***}P < 0.001$; $^{****}P < 0.0001$. **j** Cryo-EM density maps of N7-cADPR-bound *Ec*Caspase oligomers. **k** The superposition of N7-cADPR-bound *Ec*Caspase dimer, tetramer, and hexamer. **l** The zoomed-in view of the N7-cADPR-binding mode (ligand in cyan). Key interacting residues are shown as sticks. **m** Structural comparison between ligand-free and N7-cADPR-bound *Ec*Caspase. **n, o** Overall (**n**) and close-up (**o**) views of the CTD–CTD interface in the ligand-free and N7-cADPR-bound states. Interacting residues are shown as sticks. **p** Superposition of ligand-free and N7-cADPR-bound *Ec*Caspase, with the four functional loops labelled. **q** Co-immunoprecipitation analysis validating the interaction between Mhp and the *Ec*TIR protein. **r** Bacterial growth spot assays showing the expression of Mhp in cells harboring the type IV Thoeris system. "*" indicates catalytic-dead mutants. The results are representative of three independent biological experiments. **s** Schematic model illustrating the activation mechanism of the type IV Thoeris system upon phage infection.

This arrangement produces a well-ordered, spine-and-sheath-like organization of the filament. Within the dimeric asymmetric unit, the two *Ec*Caspase protomers (termed A1 and A2) associate into a domain-swapped dimer, forming three intra-dimer interfaces with a combined buried surface area of ~2,100 Å^2 (Supplementary Fig. S7a–c). The *Ec*Caspase dimers pack in a tightly arranged, side-by-side configuration to assemble into the filament. Both the NTDs and CTDs contribute to filament formation, generating two major interfaces (NTD–NTD and CTD–CTD interfaces) that together bury ~1,700 Å^2 of surface area (Supplementary Fig. S7d, e). Mutations disrupting these interfaces prevented filament formation, markedly reduced N7-cADPR binding, abolished *Ec*Caspase-mediated peptide cleavage, and completely eliminated type IV Thoeris-mediated antiphage defense, implying that filament assembly is essential for the antiviral function of the system (Fig. 1e, i; Supplementary Figs. S3e, S8).

We next determined the cryo-EM structure of MBP-fused *Ec*Caspase bound to N7-cADPR (Supplementary Fig. S9). The two-dimensional class averages revealed oligomeric particles, distinct from the supramolecular assembly observed in the ligand-free sample. The majority of particles (~60%) represent a dimeric species, whereas two additional classes corresponding to tetrameric and hexameric assemblies (each ~20%) were also observed (Fig. 1j; Supplementary Fig. S9c). However, the dimeric units among the three oligomeric states were essentially identical (Fig. 1k). It is plausible that the tetrameric and hexameric species likely represent intermediates upon N7-cADPR binding. In the N7-cADPR-bound dimeric unit, an N7-cADPR molecule nestles into an inter-protomer pocket created by the two CTDs (Fig. 1l; Supplementary Fig. S10a, b). The ligand is recognized through extensive π-stacking, hydrogen-bonding, and electrostatic interactions. Mutations disrupting the N7-cADPR-binding pocket markedly reduced *Ec*Caspase-mediated peptide cleavage and completely abolished antiphage activity, demonstrating that N7-cADPR recognition by the CTD pocket is indispensable for *Ec*Caspase-dependent peptide degradation and the antiviral defense of the type IV Thoeris system (Fig. 1e, i).

While the overall structure of the dimeric *Ec*Caspase unit in the absence of N7-cADPR resembles that of the N7-cADPR-bound dimer, the CTDs rotate outward by approximately 7 Å to accommodate N7-cADPR (Fig. 1m). Remarkably, structural superposition of the N7-cADPR-bound dimer onto the dimeric unit in the context of filamentous form reveals that N7-cADPR binding induces an outward displacement of the CTD from the A1 protomer toward the CTD from the C2 protomer, thereby leading to a steric clash between the two CTDs (Fig. 1n, o). At the same time, the CTD of A1 moves away from the CTD of the neighboring B1 protomer, disrupting the original CTD–CTD interface, including the interaction between Asp289 and Leu235, which has been shown to be critical for filament formation (Fig. 1o; Supplementary Fig. S7e). Similarly, the CTD–CTD interface is also impaired in the ligand-bound tetrameric and hexameric assemblies, with only partial NTD-mediated contacts maintaining these intermediate states (Supplementary Fig. S10c–f). Notably, Tyr295 in the CTD of A1 reorients forms a polar contact with Arg239 in the CTD of B1 to directly bind with N7-cADPR, which stabilizes its binding (Fig. 1l, o). Together, it can be concluded that N7-cADPR binding not only imposes steric hindrances that interfere with the filament formation, but also weakens the assembly interactions. These ligand-initiated conformational rearrangements may propagate throughout the filament structure and finally be coupled with the structural destabilization and subsequent depolymerization.

To test whether the CTD-mediated clash can act as a trigger for activation, we introduced the D267R/E268R double mutation to mimic the steric conflict (Supplementary Fig. S11a). The mutant exhibited almost no detectable substrate cleavage activity even in the presence of N7-cADPR (Fig. 1e), suggesting that the CTD conformational change is unlikely to serve as the primary trigger for protease activation. Instead, it more likely reflects a ligand-induced structural rearrangement within the assembled state, with ligand binding acting as the principal activation cue. Alternatively, full allosteric activation of the NTD may require both ligand engagement and disassembly.

In human caspases, four conserved loops (L1–L4) surrounding the catalytic pocket undergo rearrangement upon cleavage to form a catalytically competent enzyme[3,4]. Structural comparison revealed that *Ec*Caspase contains four corresponding loops, prompting us to compare their conformations between the ligand-free (auto-inhibited) and N7-cADPR-

bound (active) states (Fig. 1p; Supplementary Fig. S11b). The catalytic dyad adopts a conformation reminiscent of that in human caspase and is not altered upon N7-cADPR binding. Likewise, the L1, L2, and L4 loops also exhibit slight shifts in response to N7-cADPR binding, contrasting with the substantial conformation changes in human caspase. However, the L3 loop undergoes a pronounced order-to-disorder transition. In particular, L3 folds into a short helix that packs over the catalytic dyad in the filament structure. In comparison with the inhibitor/substrate-bound human caspase structure (Supplementary Fig. S11c), the helical L3 in *Ec*Caspase sterically clashes with the inhibitor/substrate. Thus, it appears that the L3 region of *Ec*Caspase occupies the inhibitor/substrate-binding site, thereby blocking substrate access and keeping *Ec*Caspase in an auto-inhibited state. Upon activation by N7-cADPR, however, the L3 region becomes highly flexible (Fig. 1p), allowing protein or peptide substrates to enter the catalytic pocket. Consistently, L3 deletion did not affect filament assembly or N7-cADPR binding but abolished N7-cADPR-dependent peptide cleavage and impaired antiphage defense (Fig. 1e, i; Supplementary Figs. S3e, S8). These observations indicate that the L3 region may function as a gating element that regulates the activation of *Ec*Caspase.

To identify phage activators, we performed a Strep pull-down assay followed by LC-MS/MS using *E. coli* expressing Strep-tagged *Ec*TIR after T6 infection (Supplementary Fig. S12a). The T6 major head protein (Mhp, a capsid protein) was identified as the most enriched *Ec*TIR-associated factor (Supplementary Fig. S12b). The *Ec*TIR-Mhp association was further validated by the *in vivo* co-immunoprecipitation assay, supporting Mhp as a strong candidate for a phage-derived activator of the type IV Thoeris system (Fig. 1q). Moreover, we also isolated T6 escape mutants on cells expressing the type IV Thoeris system and sequenced their genomes to identify the functional activators (Supplementary Fig. S13). Strikingly, all four independent escape isolates carried nonsense mutations in the *mhp* gene that result in premature termination of the major head protein. These data suggest that mutations in Mhp allow phage to bypass the Thoeris activation, providing genetic evidence that the major capsid protein is the bona fide trigger of this TIR-caspase defense pathway. Together with previous studies of type I Thoeris[5], these findings support a conserved "capsid-sensing" strategy for TIR activation across Thoeris systems. To further evaluate whether Mhp indeed activates this system, we co-expressed Mhp together with the Thoeris operon in *E. coli* (Fig. 1r). Whereas expression of either component alone was not toxic, co-expression of Mhp with the Thoeris system resulted in pronounced growth inhibition. Importantly, this toxicity was reduced when the catalytic residues of either *Ec*TIR or *Ec*Caspase were mutated, demonstrating that Mhp-induced toxicity is dependent on *Ec*TIR-catalyzed N7-cADPR synthesis and subsequent *Ec*Caspase activation.

Unlike human inflammatory and initiator caspases, which are activated through higher-order assembly[6-8], *Ec*Caspase adopts an alternative activation mechanism involving ligand-triggered assembly remodeling. Our findings suggest that the assembled filament may pre-organize neighboring CTDs into a composite pocket to enable N7-cADPR-binding, priming the complex for ligand-triggered disassembly and activation. By contrast, the isolated CTD-containing protein remains monomeric, likely because of weak intrinsic CTD–CTD interactions (Supplementary Figs. S7b, S14). Binding of a single N7-cADPR molecule at the CTD dimer interface triggers the rearrangement of the CTDs for filament depolymerization. Thus, filament formation is crucial for positioning the CTDs to accommodate N7-cADPR. Ligand binding may promote filament disassembly, releasing conformational constraints imposed by the filament architecture and enabling the structural flexibility and active-site remodeling required for protease activation. The resulting lower-order assemblies may further provide increased conformational adaptability for substrate engagement within the crowded bacterial cytoplasm.

An L3-helical element gates the catalytic core for inhibition in the *Ec*Caspase filament. Ligand-triggered depolymerization displaces L3 from the catalytic dyad and opens the catalytic pocket for substrate access, thereby activating the protease activity. Although L3 destabilization may be partly coupled to filament disassembly, disassembled oligomers alone are insufficient to support proteolytic activity (Fig. 1e), indicating that filament disassembly is not the sole determinant of L3 displacement. The precise allosteric mechanism linking ligand binding to L3 destabilization therefore remains to be fully elucidated. Assembly-dependent activation has been described for bacterial immune proteases such as the CRISPR-associated Lon-SAVED protease CalpL[9,10], whereas filament depolymerization activation remains largely unexplored. Notably, the filament depolymerization activation mechanism described here has so far been established only for *Ec*Caspase, and whether it is conserved across other type IV Thoeris systems remains unknown. Together with the recently characterized *Pseudomonas* caspase, which undergoes ligand-induced filament remodeling[11], our findings suggest that Thoeris systems employ diverse ligand-driven assembly transitions to regulate protease activation. Although native PAGE supports phage-induced *Ec*Caspase disassembly (Supplementary Fig. S3d), direct visualization of this transition *in vivo* remains challenging and will require future *in situ* approaches such as cryo-ET. Together, our findings uncover a ligand-triggered depolymerization-activation mechanism for a bacterial caspase-like protease and establish type IV Thoeris as a prototypical nucleotide immune signaling pathway that couples TIR-generated small molecules to proteolytic effector activation (Fig. 1s).

DATA AVAILABILITY

The atomic coordinates have been deposited in the Protein Data Bank under accession codes 9X0G (N7-cADPR-bound *Ec*Caspase dimer), 9X0T (N7-cADPR-bound *Ec*Caspase tetramer), 9X0U (N7-cADPR-bound *Ec*Caspase hexamer), 9X0S (MBP-fused *Ec*Caspase filament) and 27XF (*Ec*Caspase filament). Cryo-EM maps have been deposited in the Electron Microscopy Data Bank under corresponding accession codes EMD-66434, EMD-66442, EMD-66443, EMD-66441 and EMD-81533.

ACKNOWLEDGEMENTS

We thank the Core Facility of Research Center of Basic Medical Sciences in Tianjin Medical University for providing technical assistance. This work was supported by Scientific Research

Program of Tianjin Municipal Education Commission (2023ZD011), The Tianjin Key Medical Discipline (Specialty) Construction Project (TJYXZDXK-009A and TJYXZDXK-3-004B).

AUTHOR CONTRIBUTIONS

Conceptualization: X.L., H.Y., and H.Z.; Experimental studies: Q.H., B.L., Z.L., Q.Z., X.W., T.M., J.H., and F.L.; Data analysis: X.L., Q.H., B.L., Z.L., X.W., Y.L., Z.Yin, S.Z., Y.W., Z.S., Z.Yuan, H.Y., and H.Z.; Supervision: H.Z.; Manuscript writing: X.L., Z.L., and H.Z. with contributions from all authors.

COMPETING INTERESTS

The authors declare no competing interests.

REFERENCES

1. Hobbs, S.J. & Kranzusch, P.J. *Annu. Rev. Microbiol.* **78**, 255–276 (2024).
2. Rousset, F. et al. *Science* **387**, 510–516 (2025).
3. Shi, Y.G. *Cell* **117**, 855–858 (2004).
4. Riedl, S.J. et al. *Proc. Natl. Acad. Sci. USA* **98**, 14790–14795 (2001).
5. Roberts, C.G. et al. *Nat. Microbiol.* **10**, 2892–2902 (2025).
6. Park, H.H. *Int. J. Mol. Med.* **43**, 1119–1127 (2019).
7. Wein, T. et al. *Nature* **639**, 727–734 (2025).
8. Park, H.H. *Cell Death Differ.* **26**, 1213–1220 (2019).
9. Huang, P. et al. *Nat. Chem. Biol.* (2026). DOI: 10.1038/s41589-026-02252-8.
10. Smalakyte, D., Ruksenaite, A., Sasnauskas, G., Tamulaitiene, G. & Tamulaitis, G. *Mol. Cell* **84**, 4239–4255.e8 (2024).
11. Wei, L. et al. *Vita* (2026). DOI: 10.15302/vita.2026.06.0047.

ADDITIONAL INFORMATION

Supplementary information The online version contains supplementary material available at https://doi.org/10.15302/vita.2026.10.0084.

Correspondence and requests for materials should be addressed to Heng Zhang.

Reprints and permission information is available at https://www.vita-journal.com/.

© The Author(s) 2026. Published by Higher Education Press. This is an Open Access article distributed under the terms of the CC BY license (https://creativecommons.org/licenses/by/4.0/).